07.2;15.2

# Studies of the thermal conductivity and thermal resistance of solder layers with lead-free pastes by the photodeflection method

© A.L. Glazov, V.S. Kalinovskii, E.V. Kontrosh, K.L. Muratikov

Ioffe Institute, St. Petersburg, Russia
E-mail: glazov.holo@mail.ioffe.ru

Received August 11, 2022
Revised September 29, 2022
Accepted October 6, 2022

The processes of heat removal from multijunction solar cells on a germanium substrate to AlN ceramics through a solder layer were studied by thermal wave photodeflection methods. Two types lead-free solder based on SnBi and SnAgCu were used under various pressure soldering conditions. The thermal conductivity and thermal resistance of the solder layers are compared. It is shown that the thermal conductivities of the solder layers differ from the reference data for the corresponding metal alloys, and in some cases may depend on the pressure during the brazing process.

**Keywords:** thermal resistance, multi-junction solar cells, lead-free solder, non-destructive testing, thermal waves.

DOI: 10.21883/TPL.2022.11.54897.19338

The reliability and operating performance of modern semiconductor devices with a high heat release depend largely on the efficiency of heat removal [1]. Among these devices are solar batteries with solar radiation concentrators and photodetectors of laser radiation [2–4]. The heat-removing properties of such devices depend primarily on the interface (solder layer between a photovoltaic converter and a heat-removing base (HB)) quality. We have already studied the heat-removing properties of lead-containing solder joints [5–7]. It was found that the compositional uniformity of the solder layer is disturbed in the soldering process, and thermal resistances form at its boundaries, altering the heat-removing properties of the structure as a whole [7].

At the same time, various binary [8,9] and ternary [9–11] lead-free solders are now being used more and more often due to the strengthening of ecological requirements. Their thermophysical properties remain underexplored (especially in semiconductor–HB solder joints). In the present study, we report the results of examination of heat-conducting characteristics of the InGaP/Ga(In)As/Ge solar cell (SC)−solder−HB structure, which was assembled using lead-free solder pastes KOKI TB48-M742 (based on the Sn42Bi58 binary alloy [12]) and AIM REL61 M8 (made of NC258 solder based on the SnAg3Cu0.5 ternary alloy with added Bi [13]), by thermal wave photodeflection technique (PD) [5]. Samples with a size of approximately $6 \times 5$ mm were prepared to study the heat-conducting characteristics of the solder layer between multijunction (MJ) InGaP/GaAs/Ge SCs with a thickness of 150 $\mu$m and a ceramic AlN HB 250 $\mu$m in thickness. The rear contact to the *p*-Ge MJ SC substrate comprised Ag−Mg alloy layers, Ni, and the final gold layer with a thickness of 200 nm, which was deposited electrochemically. The overall thickness of this contact did not exceed 0.5 $\mu$m. The metal contact to the AlN ceramic surface was formed from a Ti sublayer onto which copper, nickel, and electrochemical gold layers were deposited in succession. The thickness of gold was no less than 1 $\mu$m. The overall thickness of this contact did not exceed 7 $\mu$m. Soldering was performed using a VS160 Budatec (Germany) system [14] in accordance with the temperature profiles specified by solder paste manufacturers [12,13]. Reflow soldering was carried out in vacuum under an initial pressure of 1 mbar. The studied samples were heated at a rate of 60°C/min to the flux activation temperature ($t = 150$°C). The temperature in the working chamber was then stabilized for approximately 2 min. After that, the samples were heated additionally to the flowing temperature (215°C) with subsequent thermal stabilization (up to 2 min). The rate of cooling to room temperature was 70°C/min. Several samples were kept under a pressure of 25, 50, and 75 g/cm$^2$ in the process of soldering.

The heat-transfer properties of solder MJ SC–HB contacts were examined using the method for determination of thermophysical parameters of multilayer objects from the direction of a surface perpendicular to the layer boundaries. This method was discussed in our earlier study [5]. To prepare the soldered MJ SC–AlN HB samples for this study, they were divided into two halves across the structure by disk cutting. Samples with different solder process parameters were arranged into a single assembly to perform measurements in one cycle. The end surface of the assembly (the cut face) was polished to class $\geqslant 9$ prior to measurements. This surface was irradiated by focused radiation of a CW solid-state laser with a wavelength of 0.532 nm modulated in time with a frequency of 1 kHz. The spot diameter on the surface was approximately 15 $\mu$m. Thermal waves induced this way in the structure were detected by measuring the deflection of a probe He−Ne laser beam

propagating over the heated surface. The detected PD signal is proportional to the angle of deflection in the direction perpendicular to the surface. If a traveling thermal wave encounters thermal resistance, the local surface temperature increases, amplifying the signal. The sample was scanned along two coordinates over the cut surface to examine the PD signal behavior. The obtained PD images were used to determine the properties of individual structure layers. Figure 1 shows the cut surface of one of the structures with AIM solder paste imaged with an optical microscope and by the PD method. The model of formation of a PD signal from multilayer objects, which was developed in our earlier study [6], was used for quantitative analysis. This model factors in both the parameters of layers and inhomogeneous boundary conditions between layers. In the present case, calculations were performed for a four-layer (germanium substrate, solder layer, copper contact, AlN ceramic material) object. The contact on the germanium surface was sufficiently thin to not be recognized as a separate layer, but gold contained in the contact alters the properties of the adjacent solder layer by dissolving in it. We have analyzed this effect thoroughly for a commonly used tin-lead solder [7]. It was also demonstrated in [7] that a change in the solder composition induces considerable variations of its thermal conductivity and thermal capacity. The latter factor may be taken into account by introducing thermal impedance [15] into the boundary condition for heat fluxes. In the discussed case of lead-free solder pastes, it was also needed to introduce a similar parameter into the Ge substrate–solder layer boundary condition to characterize the PD signal accurately. The boundary conditions for the heat transfer equation at the germanium–solder interface ($x = 0$) then take the following form:

$$T_{\mathrm{Ge}}(0,t) - T_S(0,t) = -R_t K_S \left.\frac{\partial T_S(x,t)}{\partial x}\right|_{x=0}, \qquad (1)$$

$$K_{\mathrm{Ge}} \left.\frac{\partial T_{\mathrm{Ge}}(x,t)}{\partial x}\right|_{x=0} - K_S \left.\frac{\partial T_S(x,t)}{\partial x}\right|_{x=0} = -Z_t T_S(0,t), \qquad (2)$$

where $R_t$ is the thermal resistance, $Z_t$ is the capacitive thermal conductance, and index $S$ stands for „solder“. The boundary conditions at other interfaces are assumed to be uniform.

The thermal conductivity and thickness of the solder layer, the thickness and average thermal conductivity of the solder–HB contact layer, and the thermal resistance and capacitive thermal conductance of the contact on the SC side were the adjustable parameters of the model. The key thermophysical parameters were assumed to be known: $K_{\mathrm{Ge}} = 0.67\,\mathrm{W/(cm \cdot K)}$, $(\rho C)_{\mathrm{Ge}} = 1.76\,\mathrm{J/(cm^3 \cdot K)}$, $K_{\mathrm{AlN}} = 1.8\,\mathrm{W/(cm \cdot K)}$, and $(\rho C)_{\mathrm{AlN}} = 2.4\,\mathrm{J/(cm^3 \cdot K)}$, where $K$ is the thermal conductivity, $\rho$ is the density, and $C$ is the specific thermal capacity at constant pressure. Since volumetric thermal capacity $\rho C$ of the solder layer depends only weakly on the paste composition and has a marginal effect on the approximation result, it was also fixed in the process of fitting. The layer thicknesses were monitored optically using an „Altami MET 6S“ microscope. The coordinate dependence of the signal in the direction perpendicular to the layers was approximated. In order to reduce the error due to surface irregularity, the signal was averaged along the layers.

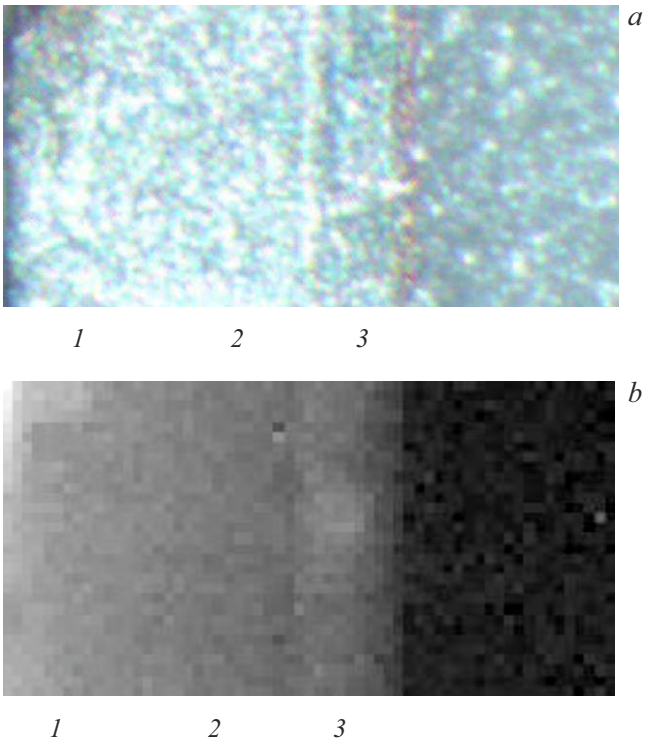


**Figure 1.** Optical ($a$) and photodeflection ($b$) images of a part of the cut surface of the SC–solder–AlN ceramic material structure. *1* — SC, *2* — solder layer, *3* — AlN ceramic material. The image size is $0.3 \times 0.15$ mm.

Figure 2 presents the dependences of amplitude of the averaged experimental signal on the distance from the Ge substrate–solder boundary and the results of approximation of these dependences. The PD signal on the MJ SC side increases in intensity due to the fact that a layer of glue is applied at the contact with the other sample. In the solder layer, the signal intensifies due to the fact that pastes have a lower thermal conductivity than Ge (and certainly than the HB).

The thermophysical characteristics of solder pastes used in the experiment are not specified by their manufacturers. Relying on literature data for similar compositions, we estimated the thermal conductivities of base alloys at $K_{\mathrm{AIM}} \sim 0.6–0.7\,\mathrm{W/(cm \cdot K)}$ and $K_{\mathrm{KOKI}} \sim 0.2\,\mathrm{W/(cm \cdot K)}$. The experimentally determined thermal conductivities of solder layers differ from these values for the corresponding alloys. The thermal conductivity of the AIM REL61 M8 solder layer is almost independent of pressure and assumes a value of $\sim 0.5\,\mathrm{W/(cm \cdot K)}$. In contrast, the thermal conductivity of the KOKI TB48-M742 solder layer increases significantly with pressure produced in the process of

soldering. Its value changes from $0.13\,W/(cm \cdot K)$ under pressureless conditions to $0.26\,W/(cm \cdot K)$ under a pressure of $75\,g/cm^2$. In all cases, $Z_t = 180 \pm 20\,W/(cm^2 \cdot K)$ at the used frequency of 1 kHz. Figure 3 presents the dependences of thermal resistance $R_{tS}$ of two types of solder layers on the pressure produced in the process of soldering. The thermal resistance of the AIM solder layer is independent of pressure and assumes a value of $\sim 0.01\,cm^2 \cdot K/W$. The thermal resistance of the KOKI solder layer decreases by a factor of about 2 (from 0.037 to $0.020\,cm^2 \cdot K/W$) as the pressure increases from 0 to $75\,g/cm^2$; however, it still remains two times higher than the AIM solder thermal resistance. Significant errors corresponding to two samples with KOKI solder in Fig. 3 are the result of a considerable spread of experimental data for these samples. It should be noted that the thermal conductivity of the AIM REL61 M8 solder layer turned out to be approximately two times higher

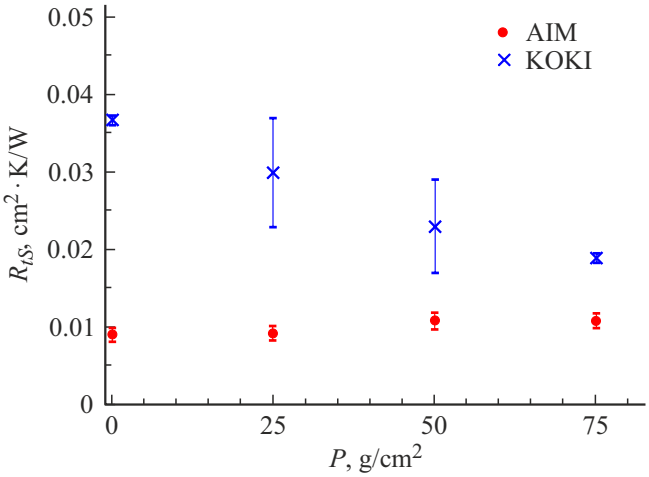


**Figure 3.** Load dependences of the thermal resistance of the solder layer corresponding to two types of solder: AIM and KOKI.

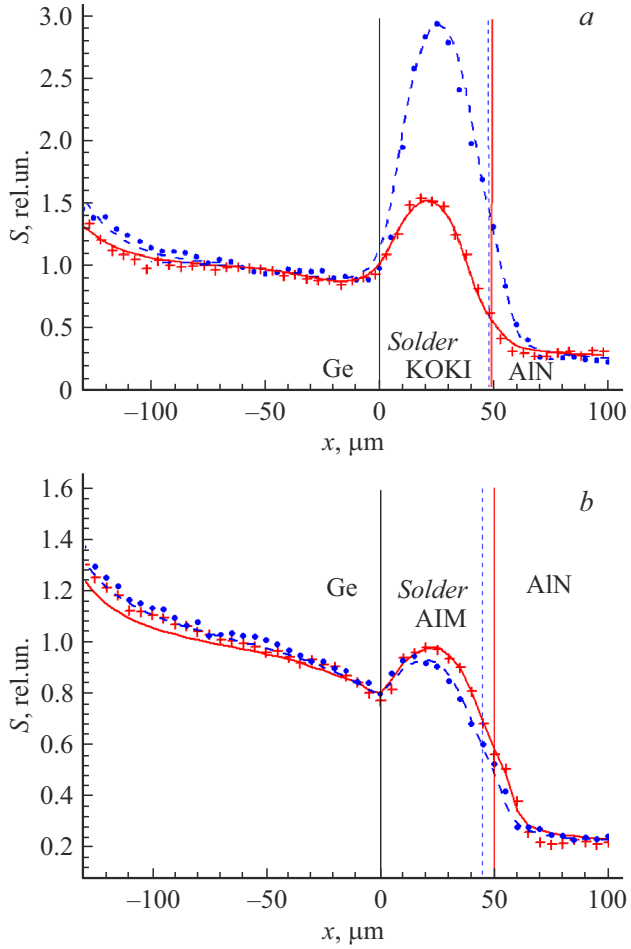


**Figure 2.** Dependences of the photodeflection signal on the distance transverse to the solder layer boundaries. *a* — KOKI solder, *b* — AIM solder. The dashed curve and circles correspond to samples soldered under pressureless conditions, while the solid curve and crosses correspond to samples soldered under a pressure of $75\,g/cm^2$. Symbols denote experimental data, and curves are the result of approximation with the five-layer sample model. Vertical straight lines of the corresponding type mark layer boundaries.

than the thermal conductivity of the lead-containing solder layer examined in [5], while the thermal conductivity of the KOKI TB48-M742 solder layer under a pressure of $75\,g/cm^2$ roughly corresponds to the value from [5].

Thus, the obtained results suggest that actual thermal characteristics of solder layers, which may differ considerably from the characteristics of base multicomponent alloys, should de taken into account in choosing the proper (i.e., providing the most efficient heat removal) solder paste and process conditions for soldering InGaP/GaAs/Ge SCs on AlN HBs.

### Conflict of interest

The authors declare that they have no conflict of interest.

## References

[1] J. Mathew, S. Krishnan, J. Electron. Packag., **144**, 010801 (2022). DOI: 10.1115/1.4050002

[2] V.S. Kalinovskii, E.V. Kotrosh, A.V. Andreeva, E.A. Ionova, A.V. Malevskaya, V.M. Andreev, V.B. Malutina-Bronskaya, V.B. Zalesskiy, A.M. Lemeshevskaya, V.I. Kuzoro, V.I. Khalimanovich, M.K. Zayceva, AIP Conf. Proc., **2149**, 030003 (2019). DOI: 10.1063/1.5124180

[3] D.F. Zaitsev, V.M. Andreev, I.A. Bilenko, A.A. Berezovskii, P.Yu. Vladislavskii, V.F. Gurfinkel', L.I. Tsvetkova, V.S. Kalinovskii, N.M. Kondrat'ev, V.N. Kosolobov, V.F. Kurochkin, S.O. Slipchenko, N.V. Smirnov, B.V. Yakovlev, Radiotekhnika, **85** (4), 153 (2021) (in Russian). DOI: 10.18127/j00338486-202104-17

[4] M. O'Neill, A.J. McDanal, M. Piszczor, M. Myers, P. Sharps, C. McPheeters, J. Steinfeldt, in *2017 IEEE 44th Photovoltaic Specialist Conf. (PVSC)* (IEEE, 2017). p. 525. DOI: 10.1109/PVSC.2017.8366596

[5] A.L. Glazov, V.S. Kalinovskii, E.V. Kontrosh, K.L. Muratikov, Tech. Phys. Lett., **42** (6), 570 (2016). DOI: 10.1134/S1063785016060080.

[6] A.L. Glazov, V.S. Kalinovskii, K.L. Muratikov, Int. J. Heat Mass Transf., **120**, 870 (2018). DOI: 10.1016/j.ijheatmasstransfer.2017.12.049
[7] A.L. Glazov, V.S. Kalinovskii, A.V. Nashchekin, K.L. Muratikov, J. Alloys Compd., **800**, 23 (2019). DOI: 10.1016/j.jallcom.2019.06.054
[8] M. Wu, J. Li, J. Electron. Mater., **47**, 155 (2018). DOI: 10.1007/s11664-017-5909-7
[9] F.Q. Hu, Q.K. Zhang, J.J. Jiang, Z.L. Song, Mater. Lett., **214**, 142 (2018). DOI: 10.1016/j.matlet.2017.11.127
[10] Y. Altintas, Y. Kaygisiz, E. Öztürk, S. Aksöz, K. Keşlioğlu, N. Maraşli, Int. J. Therm. Sci., **100**, 1 (2016). DOI: 10.1016/j.ijthermalsci.2015.09.004
[11] S. Cheng, C.-M. Huang, M. Pecht, Microelectron. Reliab., **75**, 77 (2017). DOI: 10.1016/j.microrel.2017.06.016
[12] https://www.ko-ki.ru/produktsiya/payalnye-pasty
[13] https://aim.avanteh.ru/katalog/bezotmyvnye-materialy/bezotmyvnaja-pajalnaja-pasta-m8
[14] https://budatec.ru/cat/vacuum/ustanovka-vakuumnoi-paiki-vs160ug
[15] A.L. Glazov, O.S. Vasyutinskii, Tech. Phys. Lett., **40** (12), 1130 (2014). DOI: 10.1134/S1063785014120244.